Efficient Sparse Matrix-Vector Multiplication on CUDA

Nathan Bell* and Michael Garland†

December 11, 2008

Abstract

The massive parallelism of graphics processing units (GPUs) offers tremendous performance in many high-performance computing applications. While dense linear algebra readily maps to such platforms, harnessing this potential for sparse matrix computations presents additional challenges. Given its role in iterative methods for solving sparse linear systems and eigenvalue problems, sparse matrix-vector multiplication (SpMV) is of singular importance in sparse linear algebra.

In this paper we discuss data structures and algorithms for SpMV that are efficiently implemented on the CUDA platform for the fine-grained parallel architecture of the GPU. Given the memory-bound nature of SpMV, we emphasize memory bandwidth efficiency and compact storage formats. We consider a broad spectrum of sparse matrices, from those that are well-structured and regular to highly irregular matrices with large imbalances in the distribution of nonzeros per matrix row. We develop methods to exploit several common forms of matrix structure while offering alternatives which accommodate greater irregularity.

On structured, grid-based matrices we achieve performance of 36 GFLOP/s in single precision and 16 GFLOP/s in double precision on a GeForce GTX 280 GPU. For unstructured finite-element matrices, we observe performance in excess of 15 GFLOP/s and 10 GFLOP/s in single and double precision respectively. These results compare favorably to prior state-of-the-art studies of SpMV methods on conventional multicore processors. Our double precision SpMV performance is generally two and a half times that of a Cell BE with 8 SPEs and more than ten times greater than that of a quad-core Intel Clovertown system.

1 Introduction

Sparse matrix structures arise in numerous computational disciplines, and as a result, methods for efficiently manipulating them are often critical to the performance of many applications. Sparse matrix-vector multiplication (SpMV) operations have proven to be of particular importance in computational science. They represent the dominant cost in many iterative methods for solving large-scale linear systems and eigenvalue problems that arise in a wide variety of scientific and engineering applications. The remaining part of these iterative methods (e.g the conjugate gradient method [16]), typically reduce to dense linear algebra operations that are readily handled by optimized BLAS [10] and LAPACK [1] implementations.

Modern NVIDIA GPUs are throughput-oriented manycore processors that offer very high peak computational throughput. Realizing this potential requires exposing large amounts of fine-grained parallelism and structuring computations to exhibit sufficient regularity of execution paths and memory access patterns. Recently, Volkov and Demmel [18] and Barrachina *et al.* [2] have demonstrated how to achieve significant percentages of peak floating point throughput and bandwidth on dense matrix operations. Dense operations are quite regular and are consequently often limited by floating point throughput. In contrast, sparse matrix

*nbell@nvidia.com
†mgarland@nvidia.com

NVIDIA Technical Report NVR-2008-004, Dec. 2008.
© 2008 NVIDIA Corporation. All rights reserved.

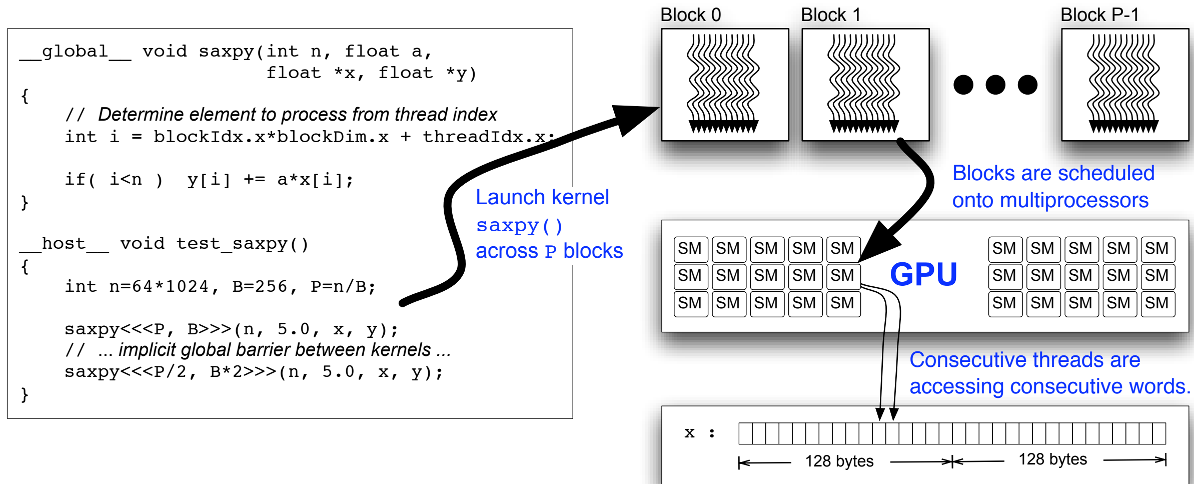

Figure 1: A saxpy kernel for computing $y \leftarrow ax + y$. Each element of the vector y is processed by one thread.

operations are typically much less regular in their access patterns and consequently are generally limited purely by bandwidth.

In this paper, we explore the design of efficient SpMV kernels for throughput-oriented processors like the GPU. We implement these kernels in CUDA and analyze their performance on the GeForce GTX 280 GPU. Sparse matrices arising in different problems can exhibit a broad spectrum of regularity. We consider data representations and implementation techniques that span this spectrum, from highly regular diagonal matrices to completely unstructured matrices with highly varying row lengths.

Despite the irregularity of the SpMV computation, we demonstrate that it can be mapped quite successfully onto the fine-grained parallel architecture employed by the GPU. For unstructured matrices, we measure performance of roughly 10 GFLOP/s in double precision and around 15 GFLOP/s in single precision. Moreover, these kernels achieve a bandwidth of roughly 90 GBytes/s, or 63.5% of peak, which indicates a relatively high level of efficiency on this bandwidth-limited computation.

2 Parallel Programming with CUDA

In the CUDA parallel programming model [13, 14], an application consists of a sequential *host* program that may execute parallel programs known as *kernels* on a parallel *device*. A kernel is a SPMD (Single Program Multiple Data) computation that is executed using a potentially large number of parallel threads. Each thread runs the same scalar sequential program. The programmer organizes the threads of a kernel into a grid of *thread blocks*. The threads of a given block can cooperate amongst themselves using barrier synchronization and a per-block shared memory space that is private to that block.

We focus on the design of kernels for sparse matrix-vector multiplication. Although CUDA kernels may be compiled into sequential code that can be run on any architecture supported by a C compiler, our SpMV kernels are designed to be run on throughput-oriented architectures in general and the NVIDIA GPU in particular. Broadly speaking, we assume that throughput-oriented architectures will provide both (1) some form of SIMD thread execution and (2) vectorized or coalesced load/store operations.

A modern NVIDIA GPU is built around an array of SM multiprocessors [12], each of which supports up to 1024 co-resident threads. A single multiprocessor is equipped with 8 scalar cores, 16384 32-bit registers, and 16KB of high-bandwidth low-latency memory. Integer and single precision floating point operations

are performed by the 8 scalar cores, while a single shared unit is used for double precision floating point operations.

Thread creation, scheduling, and management is performed entirely in hardware. High-end GPUs such as the GeForce GTX 280 or Tesla C1060 contain 30 multiprocessors, for a total possible population of 30K threads. To manage this large population of threads efficiently, the GPU employs a SIMT (Single Instruction Multiple Thread) architecture [12, 13] in which the threads of a block are executed in groups of 32 called *warps*. A warp executes a single instruction at a time across all its threads. The threads of a warp are free to follow their own execution path and all such *execution divergence* is handled automatically in hardware. However, it is substantially more efficient for threads to follow the same execution path for the bulk of the computation.

The threads of a warp are also free to use arbitrary addresses when accessing off-chip memory with load/store operations. Accessing scattered locations results in *memory divergence* and requires the processor to perform one memory transaction per thread. On the other hand, if the locations being accessed are sufficiently close together, the per-thread operations can be *coalesced* for greater memory efficiency. Global memory is conceptually organized into a sequence of 128-byte segments[1]. Memory requests are serviced for 16 threads (a half-warp) at a time. The number of memory transactions performed for a half-warp will be the number of segments touched by the addresses used by that half-warp[2]. If a memory request performed by a half-warp touches precisely 1 segment, we call this request *fully coalesced*, and one in which each thread touches a separate segment we call *uncoalesced*. If only the upper or lower half of a segment is accessed, the size of the transaction is reduced [14].

Figure 1 illustrates the basic structure of a CUDA program. The procedure `saxpy()` is a kernel entry point, indicated by the use of the `__global__` modifier. A call of the form `saxpy<<<P,B>>>` is a parallel kernel invocation that will launch `P` thread blocks of `B` threads each. These values can be set arbitrarily for each distinct kernel launch, and an implicit global barrier between kernels guarantees that all threads of the first kernel complete before any of the second are launched. When a kernel is invoked on the GPU, the hardware scheduler launches thread blocks on available multiprocessors and continues to do so as long as the necessary resources are available to do so. In this example, memory accesses to the vectors x and y are fully coalesced, since threads with consecutive thread indices access contiguous words and the vectors are aligned by the CUDA memory allocator.

Non-contiguous access to memory is detrimental to memory bandwidth efficiency and therefore the performance of memory-bound kernels. Consider the variation of the `saxpy` kernel given in Figure 2, which permits a variable *stride* between elements. Any stride greater than one results in non-contiguous access to the `x` and `y` vectors. Since larger strides result in a single warp touching more segments, we expect an inverse relationship between stride and performance of the memory-bound `saxpy` kernel. Figure 3 confirms this assumption, demonstrating that the effective memory bandwidth (and hence performance) decreases as the stride increases from 1 to 33. Memory accesses with unit stride are more than ten times faster than those with greater separation. Observe that performance of the double precision `daxpy` kernel follows a similar relationship. Also note that, for large strides, the double precision kernel achieves roughly twice the bandwidth of `saxpy`.

The relaxed coalescing rules of the GTX 200-series of processors largely mitigate the effect of alignment on memory efficiency. For example, the rate of contiguous but unaligned memory access is roughly one-tenth that of aligned access on the G80 architecture. However, on our target platform, unaligned access is approximately 60% of the aligned case, a six-fold improvement over G80. Nevertheless, ensuring proper memory alignment is key to achieving high SpMV performance.

3 Sparse Matrix Formats

There are a multitude of sparse matrix representations, each with different storage requirements, computational characteristics, and methods of accessing and manipulating entries of the matrix. Since, in the context

[1] Access granularities below 32 bits have different segment sizes [14].

[2] Earlier devices that do not support Compute Capability 1.2 have stricter coalescing requirements [14].

```
__global__
void saxpy_with_stride(int n, float a, float * x, float * y, int stride)
{
    int i = blockIdx.x * blockDim.x + threadIdx.x;

    if (i < n)
        y[i * stride] = a * x[i * stride] + y[i * stride];
}
```

Figure 2: A `saxpy` kernel with variable stride.

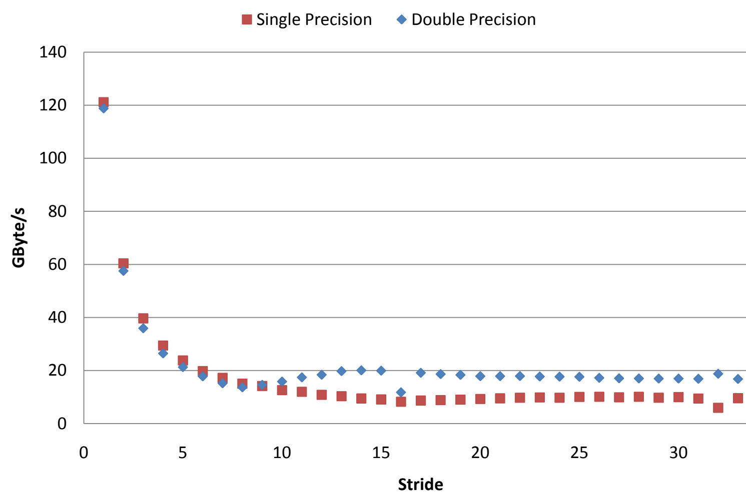

Figure 3: Relationship between stride and memory bandwidth in the `saxpy` and `daxpy` kernels.

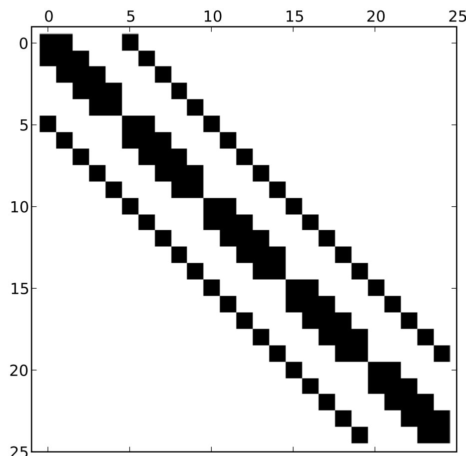

Figure 4: A 25-by-25 sparse matrix with 5 occupied diagonals. The matrix represents a finite-difference approximation to the Laplacian operator on a 5-by-5 mesh.

of sparse matrix-vector multiplication, we are not concerned with modifying matrices, we will only consider static sparse matrix formats, as opposed to those suitable for rapid insertion and deletion of elements.

The primary distinction among sparse matrix representations is the sparsity pattern, or the structure of the nonzero entries, for which they are best suited. Although sparse formats tailored for highly specific classes of matrices are the most computationally attractive, it is also important to consider *general* storage schemes which efficiently store matrices with arbitrary sparsity patterns. In the remainder of this section we summarize several sparse matrix representations and discuss their associated tradeoffs. Section 4 will then describe CUDA *kernels* for performing SpMV operations with each sparse matrix format.

3.1 Diagonal Format

When nonzero values are restricted to a small number of matrix diagonals, the *diagonal* format (DIA) is an appropriate representation [16]. Although not a general purpose format, the diagonal storage scheme efficiently encodes matrices arising from the application of stencils to regular grids, a common discretization method. Figure 4 illustrates the sparsity pattern of a 25-by-25 matrix with 5 occupied diagonals.

The diagonal format is formed by two arrays: `data`, which stores the nonzero values, and `offsets`, which stores the offset of each diagonal from the main diagonal. By convention, the main diagonal corresponds to offset 0, while $i > 0$ represents the i-th super-diagonal and $i < 0$ the i-th sub-diagonal. Figure 5 illustrates the DIA representation of an example matrix with three occupied diagonals. In our implementation, `data` is stored in column-major order so that its linearization in memory places consecutive elements within each diagonal adjacently. Entries marked with the symbol $*$ are used for padding and may store an arbitrary value.

The benefits of the diagonal format are twofold. First, the row and column indices of each nonzero entry are implicitly defined by their position within a diagonal and the corresponding offset of the diagonal. Implicit indexing both reduces the memory footprint of the matrix and decreases the amount of data transferred during a SpMV operation. Second, all memory access to `data`, `x`, and `y` is contiguous, which improves the efficiency of memory transactions.

The downsides of the diagonal format are also evident. DIA allocates storage of values “outside” the matrix and explicitly stores zero values that occur in occupied diagonals. Within the intended application

$$\mathtt{A} = \begin{bmatrix} 1 & 7 & 0 & 0 \\ 0 & 2 & 8 & 0 \\ 5 & 0 & 3 & 9 \\ 0 & 6 & 0 & 4 \end{bmatrix}$$

$$\mathtt{data} = \begin{bmatrix} * & 1 & 7 \\ * & 2 & 8 \\ 5 & 3 & 9 \\ 6 & 4 & * \end{bmatrix} \qquad \mathtt{offsets} = \begin{bmatrix} -2 & 0 & 1 \end{bmatrix}$$

Figure 5: Arrays `data` and `offsets` comprise the DIA representation of `A`.

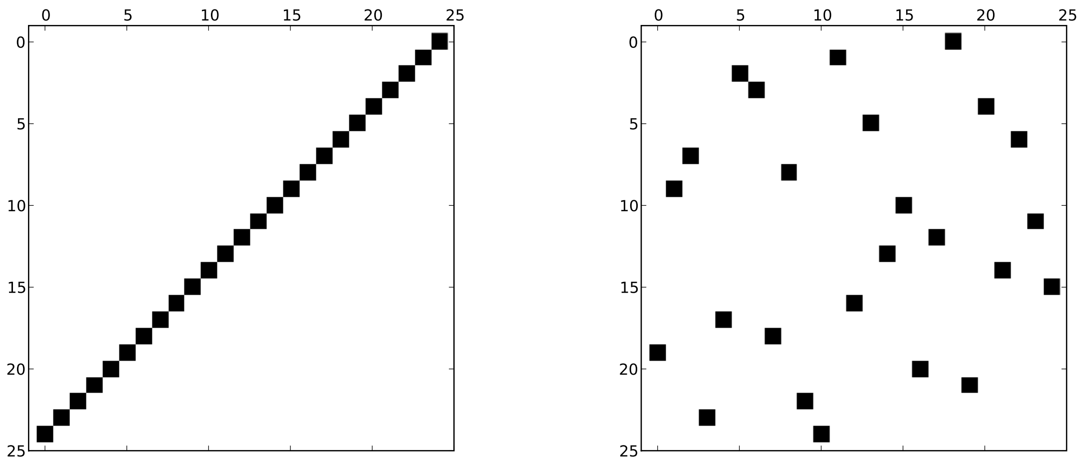

Figure 6: Sparsity patterns that are ill-suited to the sparse diagonal format.

area, i.e. stencils applied to regular grids, these are not problematic. However, it is important to note that many matrices have sparsity patterns that are inappropriate for DIA, such as those illustrated in Figure 6.

3.2 ELLPACK Format

Another storage scheme that is well-suited to vector architectures is the ELLPACK (ELL) format[3] [7]. For an M-by-N matrix with a maximum of K nonzeros per row, the ELLPACK format stores the nonzero values in a dense M-by-K array `data`, where rows with fewer than K nonzeros are zero-padded. Similarly, the corresponding column indices are stored in `indices`, again with zero, or other some sentinel value used for padding. ELL is more general than DIA since the nonzero columns need not follow any particular pattern. Figure 7 illustrates the ELLPACK representation of an example matrix with a maximum of three nonzeros per row. As in the DIA format, `data` and `indices` are stored in column-major order.

When the maximum number of nonzeros per row does not substantially differ from the average, the ELL format is an efficient sparse matrix representation. Note that row indices are implicitly defined (like DIA),

[3] Also called the ITPACK format

$$\texttt{A} = \begin{bmatrix} 1 & 7 & 0 & 0 \\ 0 & 2 & 8 & 0 \\ 5 & 0 & 3 & 9 \\ 0 & 6 & 0 & 4 \end{bmatrix}$$

$$\texttt{data} = \begin{bmatrix} 1 & 7 & * \\ 2 & 8 & * \\ 5 & 3 & 9 \\ 6 & 4 & * \end{bmatrix} \qquad \texttt{indices} = \begin{bmatrix} 0 & 1 & * \\ 1 & 2 & * \\ 0 & 2 & 3 \\ 1 & 3 & * \end{bmatrix}$$

Figure 7: Arrays `data` and `indices` comprise the ELL representation of `A`.

while column indices are stored explicitly. Aside from matrices defined by stencil operations on regular grids (for which DIA is more appropriate), matrices obtained from semi-structured meshes and especially well-behaved unstructured meshes meet this criterion. Figure 8 illustrates semi-structured and unstructured meshes which are appropriate for the ELL storage scheme.

In practice, unstructured meshes do not always meet this requirement. Indeed, as Figure 9 illustrates, the ratio between the maximum number of nonzeros per row and the average may be arbitrarily large. Clearly the ELL format alone is an inappropriate choice for representing matrices obtained from such meshes. However, a hybrid format that combines ELL with another, more general, storage scheme provides a useful alternative. We discuss one such combination in Section 3.5.

3.3 Coordinate Format

The *coordinate* (COO) format[4] is a particularly simple storage scheme. The arrays: `row`, `col`, and `data` store the row indices, column indices, and values, respectively, of the nonzero matrix entries. COO is a *general* sparse matrix representation since, for an arbitrary sparsity pattern, the required storage is always proportional to the number of nonzeros. Unlike DIA and ELL, both row and column indices are stored explicitly in COO. Figure 10 illustrates the COO representation of an example matrix. In our implementation, the `row` array is sorted, ensuring that entries with the same row index are stored contiguously.

3.4 Compressed Sparse Row Format

The *compressed sparse row* (CSR) format[5] is a popular, general-purpose sparse matrix representation. Like the COO format, CSR explicitly stores column indices and nonzero values in arrays `indices` and `data`. A third array of row pointers, `ptr`, takes the CSR representation. For an M-by-N matrix, `ptr` has length $M+1$ and stores the offset into the i-th row in `ptr[i]`. The last entry in `ptr`, which would otherwise correspond to the $(M+1)$-st row, stores NNZ, the number of nonzeros in the matrix. Figure 11 illustrates the CSR representation of an example matrix.

The CSR format may be viewed as a natural extension of the (sorted) COO representation discussed in Section 3.3 with a simple compression scheme applied to the (often repeated) row indices. As a result, converting between COO and CSR is straightforward and efficient. Aside from reducing storage, row pointers facilitate fast querying of matrix values and allow other quantities of interest, such as the number of nonzeros in a particular row (`ptr[i+1] - ptr[i]`), to be readily computed. For these reasons, the compressed row format is commonly used for sparse matrix computations (e.g., sparse matrix-matrix multiplication) in addition to sparse matrix-vector multiplication, the focus of this paper.

[4] Also called the triplet or IJV format.
[5] Also known as *compressed row storage* CRS

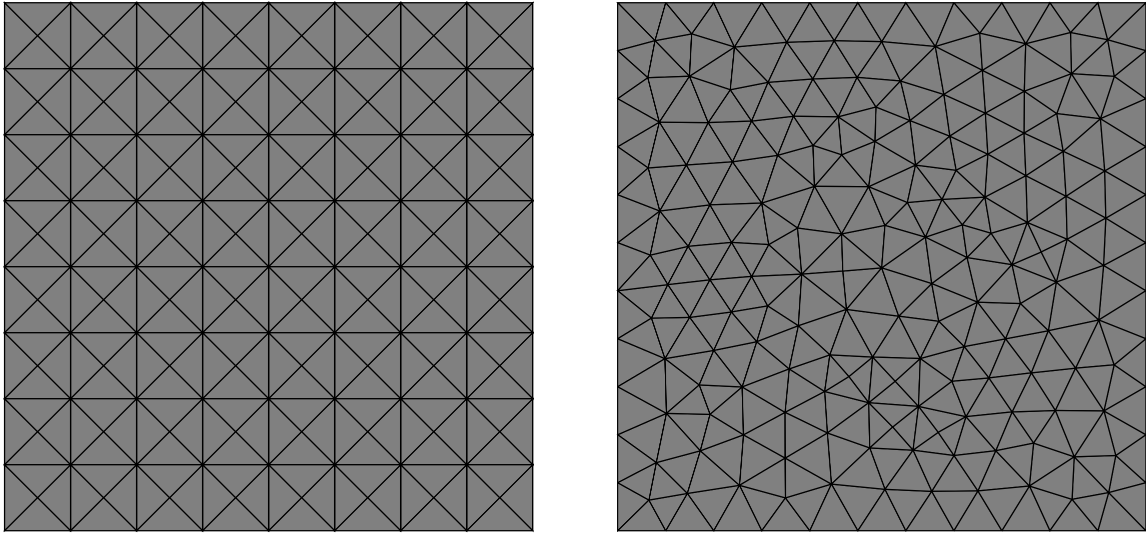

Figure 8: Example semi-structured (left) and unstructured (right) meshes whose vertex-edge connectivity is efficiently encoded in ELL format. In each case the maximum vertex degree is not significantly greater than the average degree.

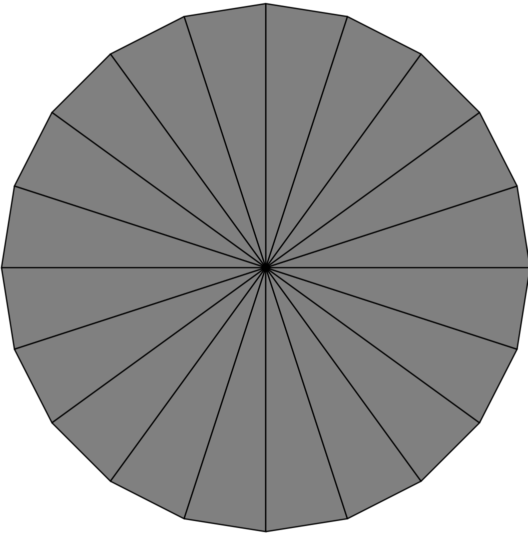

Figure 9: The vertex-edge connectivity of the wheel is not efficiently encoded in ELL format. Since the center vertex has high degree relative to the average degree, the vast majority of the entries in the `data` and `indices` arrays of the ELL representation will be wasted.

$$\texttt{A} = \begin{bmatrix} 1 & 7 & 0 & 0 \\ 0 & 2 & 8 & 0 \\ 5 & 0 & 3 & 9 \\ 0 & 6 & 0 & 4 \end{bmatrix}$$

$$\begin{aligned} \texttt{row} &= \begin{bmatrix} 0 & 0 & 1 & 1 & 2 & 2 & 2 & 3 & 3 \end{bmatrix} \\ \texttt{col} &= \begin{bmatrix} 0 & 1 & 1 & 2 & 0 & 2 & 3 & 1 & 3 \end{bmatrix} \\ \texttt{data} &= \begin{bmatrix} 1 & 7 & 2 & 8 & 5 & 3 & 9 & 6 & 4 \end{bmatrix} \end{aligned}$$

Figure 10: Arrays `row`, `col`, and `data` comprise the COO representation of `A`.

$$\texttt{A} = \begin{bmatrix} 1 & 7 & 0 & 0 \\ 0 & 2 & 8 & 0 \\ 5 & 0 & 3 & 9 \\ 0 & 6 & 0 & 4 \end{bmatrix}$$

$$\begin{aligned} \texttt{ptr} &= \begin{bmatrix} 0 & 2 & 4 & 7 & 9 \end{bmatrix} \\ \texttt{indices} &= \begin{bmatrix} 0 & 1 & 1 & 2 & 0 & 2 & 3 & 1 & 3 \end{bmatrix} \\ \texttt{data} &= \begin{bmatrix} 1 & 7 & 2 & 8 & 5 & 3 & 9 & 6 & 4 \end{bmatrix} \end{aligned}$$

Figure 11: Arrays `ptr`, `indices`, and `data` comprise the CSR representation of `A`.

3.5 Hybrid Format

While the ELLPACK format (cf. Section 3.2) is well-suited to vector architectures, its efficiency rapidly degrades when the number of nonzeros per matrix row varies. In contrast, the storage efficiency of the coordinate format (cf. Section 3.3) is invariant to the distribution of nonzeros per row. Furthermore, as we'll show in Section 4, this invariance extends to the cost of a sparse matrix-vector product using the coordinate format. Since the best-case SpMV performance of ELL exceeds that of COO, a hybrid ELL/COO format, which stores the majority of matrix entries in ELL and the remaining entries COO, is of substantial utility.

Consider a matrix that encodes the vertex connectivity of a planar triangle mesh in two dimensions. While, as Figure 9 illustrates, the maximum vertex degree of such a mesh is arbitrarily large, the *average* vertex degree is bounded by topological invariants. Therefore, the vast majority of vertices in a typical planar triangle mesh will have approximately 6 neighbors, irrespective of the presence of vertices with exceptional degree. Since similar properties hold for unstructured meshes in higher dimensions, it is worthwhile to examine sparse matrix storage schemes that exploit this knowledge.

The purpose of the hybrid format is to store the *typical* number of nonzeros per row in the ELL data structure and the remaining entries of *exceptional* rows in the COO format. Often the typical number of nonzeros per row is known a priori, as in the case of planar meshes, and the ELL portion of the matrix is readily extracted. However, in the general case this number must be determined directly from the input matrix. Our implementation computes a histogram of the row sizes and determines the the largest number K such that using K columns per row in the ELL portion of the HYB matrix meets a certain objective measure. Based on empirical results, we assume that the fully-occupied ELL format is roughly three times faster than COO. Under this modeling assumption, it is profitable to add a K-th column to the ELL structure if at least one third of the matrix rows contain K (or more) nonzeros. When the population of rows with K or more nonzero values falls below this threshold, the remaining nonzero values are placed into COO.

3.6 Packet Format

The *packet* format (PKT) is a novel sparse matrix representation designed for vector architectures. Tailored for symmetric mesh-based matrices, such as those arising in FEM discretizations, the packet format first decomposes the matrix into a given number of fixed-size partitions. Each partition is then stored in a specialized *packet* data structure.

Figure 12 shows a triangle mesh with 11 vertices and partitioning of the vertices into two sets. The objective of the partitioner is to minimize the edge cut: the total number of edges crossing between partitions. In the context of the packet format, edges within a partition correspond to values that are cached in a low-latency local memory, while the cut-edges correspond to values that must be fetched from off-chip memory. Therefore, minimizing the edge cut reduces the number of high-latency memory accesses during a SpMV operation.

Figure 13 illustrates the sparsity structure of the matrix associated with the mesh in Figure 12. Reordering rows and columns by partition number ensures that most nonzeros lie in submatrices near the diagonal. Since each submatrix contains only a small number of contiguous columns, the corresponding entries from the `x` vector can be cached in local memory. Specifically, when performing the product `A[i,j] * x[j]`, the value of `x[j]` can be precached, and then fetched from low-latency local memory rather than high-latency main memory. For now, we ignore the nonzero entries lying outside the diagonal submatrices and concentrate on representing individual submatrices compactly.

In our implementation, the partition size is bounded by a constant determined by the available local memory[6]. As a result, row and column indices within each diagonal submatrix are more compactly represented as local offsets from the first row and column of the submatrix. For example, the matrix entry $(9, 7)$ within the second submatrix is stored as an offset of $(3, 2)$ from $(6, 6)$, the base index of the submatrix. We represent the offset indices with 16-bit integers.

With submatrix indices stored as local offsets from a base index, the task remains to arrange these values in a manner suitable for SIMT execution. We consider the case where each row of the submatrix is assigned

[6]At most 2,000 vertices per partition for single-precision and 1,000 for double-precision floating-point values

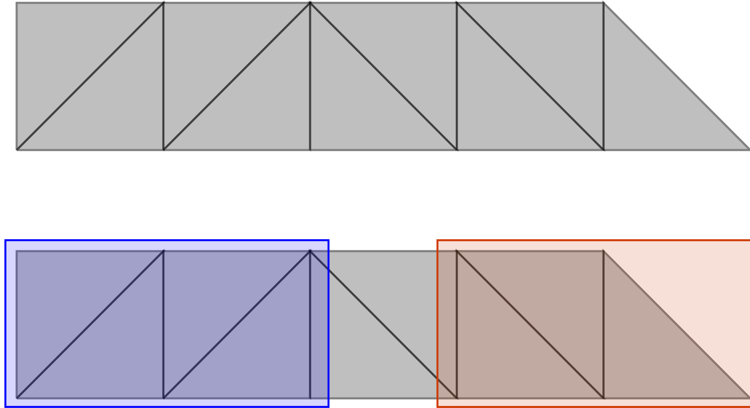

Figure 12: A sample triangle mesh with 11 vertices partitioned into two sets.

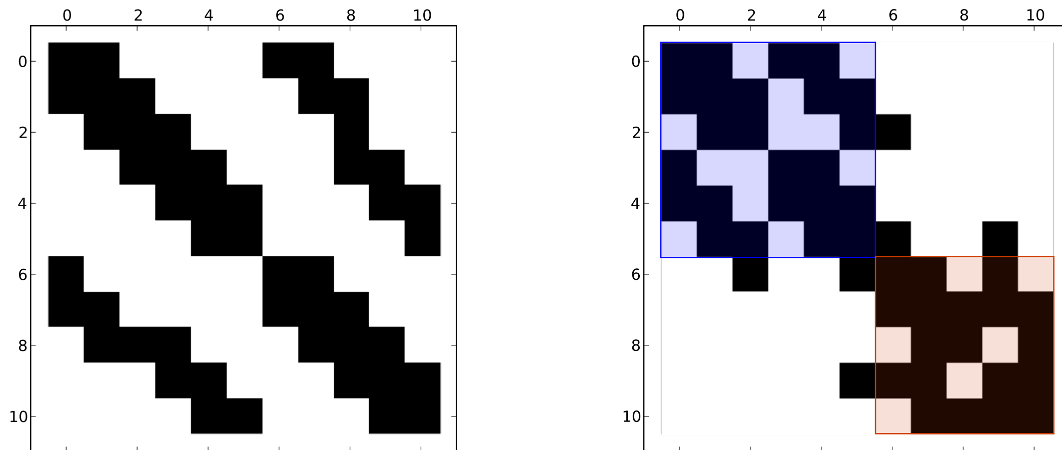

Figure 13: Reordering rows and columns by partition concentrates nonzeros into diagonal submatrices.

$$\texttt{pkt0} = \begin{bmatrix} (0,0) & (0,1) & (0,3) & (0,4) & * & * & * & * \\ (1,0) & (1,1) & (1,2) & (1,4) & (1,5) & * & * & * \\ (2,1) & (2,2) & (2,5) & (4,0) & (4,1) & (4,3) & (4,4) & (4,5) \\ (3,0) & (3,3) & (3,4) & (5,1) & (5,2) & (5,4) & (5,5) & * \end{bmatrix}$$

$$\texttt{pkt1} = \begin{bmatrix} (0,0) & (0,1) & (0,3) & (4,1) & (4,2) & (4,3) & (4,4) \\ (1,0) & (1,1) & (1,2) & (1,3) & (1,4) & * & * \\ (2,1) & (2,2) & (2,4) & * & * & * & * \\ (3,0) & (3,1) & (3,3) & (3,4) & * & * & * \end{bmatrix}$$

Figure 14: Packet storage for the two diagonal submatrices in Figure 13. The first submatrix has base index $(0, 0)$ while the second submatrix begins at $(6, 6)$. Rows of the `pkt0` and `pkt1` correspond to individual thread lanes.

to a single thread, with a fixed number of threads associated to each packet. Under these assumptions, data arrangement reduces to a packing problem: assign rows to threads such that the maximum work assigned to any thread is minimized. Although this *minimum multiprocessor scheduling* problem is NP-hard [11], we find that simple packing heuristics suffice for the domain of interest. Figure 14 illustrates packed representations of the two submatrices in Figure 13 using four threads and a greedy least-occupied-bin-first packing strategy. The nonzero values corresponding to each submatrix entry are stored in a similar fashion, either in a separate array or together with the indices. In the complete data structure, packets are concatenated together sequentially into an array of packets. In this example, the array `[pkt0, pkt1]` combines the two packets. As with the DIA and ELL formats, the packet array is stored in column-major order so concurrently executing threads access memory contiguously.

Like the coordinate portion of the hybrid ELL/COO format, nonzero matrix entries that lie outside the diagonal submatrices may be stored in a separate data structure. Alternatively, these entries may be packed in the same manner as the submatrix entries, albeit without the benefit of compressed indices. Since such entries are relatively few in number, their handling has little impact on the overall performance.

Both ELL and PKT statically schedule work on a per-thread basis. In ELL the schedule is trivial: each thread is assigned exactly one matrix row. The packet format is more general, allowing several rows to share the same thread of execution. With a reasonable scheduling heuristic, this flexibility mitigates mild load imbalances that are costly to store in ELL format.

In many ways the construction of the packet format resembles the strategy used in SpMV operations on distributed memory systems. In either case, the matrix is partitioned into pieces based on the size of the local memory store on each “node”. In our case, the individual multiprocessors on a single chip and shared memory are the nodes and local store, while in distributed systems these are conventional computers and their associated main memory. Although on different scales, the objective is to replace (relatively) high latency communication with low latency memory access.

3.7 Other Formats

The formats discussed in this section represent only a small portion the complete space of sparse matrix representations. Of these alternative formats, many are derived directly from one of the presented formats (e.g., modified CSR [15]). Others, like CSR with permutation or the jagged diagonal format [6] are natural generalizations of a basic format. Hybrid combinations of structured and unstructured formats, such as DIA and CSR [15], are also useful.

```
__global__ void
spmv_dia_kernel(const int num_rows,
                const int num_cols,
                const int num_diags,
                const int   * offsets,
                const float * data,
                const float * x,
                      float * y)
{
    int row = blockDim.x * blockIdx.x + threadIdx.x;

    if(row < num_rows){
        float dot = 0;

        for(int n = 0; n < num_diags; n++){
            int   col = row + offsets[n];
            float val = data[num_rows * n + row];

            if(col >= 0 && col < num_cols)
                dot += val * x[col];
        }

        y[row] += dot;
   }
}
```

Figure 15: SpMV kernel for the DIA sparse matrix format.

4 Sparse Matrix-Vector Multiplication

Sparse matrix-vector multiplication (SpMV) is arguably the most important operation in sparse matrix computations. Iterative methods for solving large linear systems ($Ax = b$) and eigenvalue problems ($Ax = \lambda x$) generally require hundreds if not thousands of matrix-vector products to reach convergence. In this paper, we consider the operation $y = Ax + y$ where A is large and sparse and x and y are column vectors. While not a true analog of the BLAS `gemv` operation (i.e., $y = \alpha Ax + \beta y$), our routines are easily generalized. We choose this SpMV variant because it isolates the sparse component of the computation from the dense component. Specifically, the number of floating point operations in $y = Ax + y$ is always twice the number of nonzeros in A (one multiply and one add per element), independent of the matrix dimensions. In contrast, the more general form also includes the influence of the vector operation βy, which, when the matrix has few nonzeros per row, will substantially skew performance.

In this section we describe SpMV implementations, or computational *kernels*, for the sparse matrix formats introduced in Section 3. While the following CUDA code samples have been simplified for illustrative purposes, the essence of the true implemention is maintained. For instance, the presented kernels ignore range limits on grid dimensions e.g., `gridDim.x` ≤ 65535, which complicate the mapping of blocks and threads to the appropriate indices. We refer interested readers to the source code which accompanies this paper for further implementation details.

As discussed in Section 2, execution and memory divergence are the principal considerations. Therefore, when mapping SpMV to the GPU, our task is to minimize the number of independent paths of execution and leverage coalescing when possible. While these themes are broadly applicable, our primary focus is the development of efficient kernels for CUDA-enabled devices. In particular, we target the GTX 200-series of processors which support double precision floating point arithmetic [14].

4.1 DIA kernel

Parallelizing SpMV for the diagonal format is straightforward: one thread is assigned to each row of the matrix. In Figure 15, each thread first computes a sequential thread index, `row`, and then computes the (sparse) dot product between the corresponding matrix row and the `x` vector.

Recall from Section 3.1 that the `data` the array of the DIA format is stored in column-major order. As

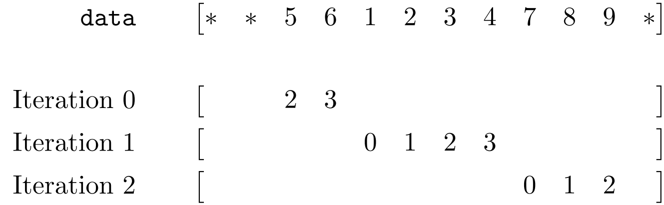

Figure 16: Linearization of the DIA `data` array and the memory access pattern of the DIA SpMV kernel.

```
__global__ void
spmv_ell_kernel(const int num_rows,
                const int num_cols,
                const int num_cols_per_row,
                const int   * indices,
                const float * data,
                const float * x,
                      float * y)
{
    int row = blockDim.x * blockIdx.x + threadIdx.x;

    if(row < num_rows){
        float dot = 0;

        for(int n = 0; n < num_cols_per_row; n++){
            int   col = indices[num_rows * n + row];
            float val = data[num_rows * n + row];

            if(val != 0)
                dot += val * x[col];
        }

        y[row] += dot;
    }
}
```

Figure 17: SpMV kernel for the ELL sparse matrix format.

Figure 16 illustrates, this linearization of the DIA `data` array ensures that threads within the same warp access memory contiguously. Since the DIA format for this matrix has three diagonals (i.e., `num_diags` = 3) the `data` array is accessed three times by each of the four executing threads. Given that consecutive rows, and hence threads, correspond to consecutive matrix columns, threads within the same warp access the `x` vector contiguously as well. As presented, memory accesses to `data` and `x` are contiguous, but not generally aligned to any specific multi-word boundary. Fortunately, aligned access to `data` is easily achieved by padding the columns of `data` (cf. Figure 5). Our implementation (not shown) uses this modification to the standard DIA data structure. Additionally, our implementation of the DIA kernel accesses values in the `offsets` array only once per block, as opposed to the per-thread access shown in Figure 15.

4.2 ELL Kernel

Figure 17 illustrates the ELL kernel which, like DIA, uses one thread per matrix row to parallelize the computation. The structure of the ELL kernel is nearly identical to that of the DIA kernel, with the exception that column indices are explicit in ELL and implicit in DIA. Therefore, the DIA kernel will generally perform better than the ELL kernel on matrices that are efficiently stored in DIA format.

The memory access pattern of the ELL kernel, shown in Figure 16, resembles that of the DIA method. Since `data` and `indices` of the ELL format are accessed in the same way we show only one access pattern. As with DIA, our implementation used padding to align the ELL arrays appropriately. However, unlike DIA,

$$
\begin{array}{rl}
\texttt{data} & \begin{bmatrix}1 & 2 & 5 & 6 & 7 & 8 & 3 & 4 & * & * & 9 & *\end{bmatrix} \\
\texttt{indices} & \begin{bmatrix}0 & 1 & 0 & 1 & 1 & 2 & 2 & 3 & * & * & 3 & *\end{bmatrix} \\
 & \\
\text{Iteration 0} & \begin{bmatrix}0 & 1 & 2 & 3 & & & & & & & & \end{bmatrix} \\
\text{Iteration 1} & \begin{bmatrix} & & & & 0 & 1 & 2 & 3 & & & & \end{bmatrix} \\
\text{Iteration 2} & \begin{bmatrix} & & & & & & & & 0 & 1 & 2 & 3\end{bmatrix}
\end{array}
$$

Figure 18: Linearization of the ELL `data` and `indices` arrays and the memory access pattern of the ELL SpMV kernel.

```
__host__ void
spmv_csr_serial(const int num_rows,
                const int   * ptr,
                const int   * indices,
                const float * data,
                const float * x,
                      float * y)
{

    for(int row = 0; i < num_rows; i++){
        float dot = 0;

        int row_start = ptr[row];
        int row_end   = ptr[row+1];

        for (int jj = row_start; jj < row_end; jj++)
            dot += data[jj] * x[indices[jj]];

        y[row] += dot;
    }
}
```

Figure 19: Serial CPU SpMV kernel for the CSR sparse matrix format.

the ELL kernel does not necessarily access the `x` vector contiguously.

4.3 CSR kernel

Consider the serial CPU kernel for the CSR format shown in Figure 19. Since the (sparse) dot product between a row of the matrix and `x` may be computed independently of all other rows, the CSR SpMV operation is easily parallelized. Figure 20 demonstrates a straightforward CUDA implementation, again using one thread per matrix row. Several variants of this approach are documented in [13], which we refer to as the *scalar* kernel.

While the scalar kernel exhibits fine-grained parallelism, its performance suffers from several drawbacks. The most significant among these problems is the manner in which threads within a warp access the CSR `indices` and `data` arrays. While the column indices and nonzero values for a given row are stored contiguously in the CSR data structure, these values are not accessed simultaneously. Instead, each thread reads the elements of its row sequentially, producing the pattern shown in Figure 21.

An alternative to the scalar method, which we call the *vector* kernel, assigns one *warp* to each matrix row. An implementation of this described in Figure 22. The vector kernel can be viewed as an application of the vector strip mining pattern to the sparse dot product computed for each matrix row. Unlike the previous CUDA kernels, which all used one thread per matrix row, the CSR vector kernel requires coordination among threads within the same warp. Specifically, a warp-wide parallel reduction is required to sum the per-thread

```
__global__ void
spmv_csr_scalar_kernel(const int num_rows,
                       const int   * ptr,
                       const int   * indices,
                       const float * data,
                       const float * x,
                             float * y)
{
    int row = blockDim.x * blockIdx.x + threadIdx.x;

    if(row < num_rows){
        float dot = 0;

        int row_start = ptr[row];
        int row_end   = ptr[row+1];

        for (int jj = row_start; jj < row_end; jj++)
            dot += data[jj] * x[indices[jj]];

        y[row] += dot;
    }
}
```

Figure 20: SpMV kernel for the CSR sparse matrix format using one thread per matrix row.

`indices`	0	1	1	2	0	2	3	1	3
`data`	1	7	2	8	5	3	9	6	4
Iteration 0	0		1		2			3	
Iteration 1		0		1		2			3
Iteration 2							2		

Figure 21: CSR arrays `indices` and `data` and the memory access pattern of the scalar CSR SpMV kernel.

```
__global__ void
spmv_csr_vector_kernel(const int num_rows,
                       const int   * ptr,
                       const int   * indices,
                       const float * data,
                       const float * x,
                             float * y)
{
    __shared__ float vals[];

    int thread_id = blockDim.x * blockIdx.x + threadIdx.x;  // global thread index
    int warp_id   = thread_id / 32;                         // global warp index
    int lane      = thread_id & (32 - 1);                   // thread index within the warp

    // one warp per row
    int row  = warp_id;

    if (row < num_rows){
        int row_start = ptr[row];
        int row_end   = ptr[row+1];

        // compute running sum per thread
        vals[threadIdx.x] = 0;
        for(int jj = row_start + lane; jj < row_end; jj += 32)
            vals[threadIdx.x] += data[jj] * x[indices[jj]];

        // parallel reduction in shared memory
        if (lane < 16) vals[threadIdx.x] += vals[threadIdx.x + 16];
        if (lane <  8) vals[threadIdx.x] += vals[threadIdx.x +  8];
        if (lane <  4) vals[threadIdx.x] += vals[threadIdx.x +  4];
        if (lane <  2) vals[threadIdx.x] += vals[threadIdx.x +  2];
        if (lane <  1) vals[threadIdx.x] += vals[threadIdx.x +  1];

        // first thread writes the result
        if (lane == 0)
            y[row] += vals[threadIdx.x];
    }
}
```

Figure 22: SpMV kernel for the CSR sparse matrix format using one 32-thread warp per matrix row.

results together.

The vector kernel accesses `indices` and `data` contiguously, and therefore overcomes the principal deficiency of the scalar approach. Memory access in Figure 23 are labeled by warp index (rather than iteration number) since the order in which different warps access memory is undefined and indeed, unimportant for performance considerations. In this example, no warp iterates more than once while reading the CSR arrays since no row has more than 32 nonzero values. Note that when a row consists of more than 32 nonzeros, the order of summation differs from that of the scalar kernel.

Unlike DIA and ELL, the CSR storage format permits a variable number of nonzeros per row. While CSR efficiently represents a broader class of sparse matrices, this additional flexibility introduces *thread divergence*. For instance, when `spmv_csr_scalar_kernel` is applied to a matrix with a highly variable number of nonzeros per row, it is likely that many threads within a warp will remain idle while the thread with the longest row continues iterating. Matrices whose distribution of nonzeros per row follows a *power law* distribution are particularly troublesome for the scalar kernel. Since warps execute independently, this form of thread divergence is less pronounced in `spmv_csr_vector_kernel`. On the other hand, efficient execution of the vector kernel demands that matrix rows contain a number of nonzeros greater than the warp size (32). As a result, performance of the vector kernel is sensitive to matrix row size.

4.4 COO Kernel

Recall from Sections 3.1 and 3.2 that the DIA and ELL formats only represent specific sparsity patterns efficiently. The CSR format is more general than DIA and ELL, however our CSR kernels suffer from thread

$$
\begin{array}{rl}
\texttt{indices} & [0\ \ 1\ \ 1\ \ 2\ \ 0\ \ 2\ \ 3\ \ 1\ \ 3] \\
\texttt{data} & [1\ \ 7\ \ 2\ \ 8\ \ 5\ \ 3\ \ 9\ \ 6\ \ 4] \\
\\
\text{Warp } 0 & [0\ \ 0\ \ \ \ \ \ \ \ \ \ \ \ \ \ ] \\
\text{Warp } 1 & [\ \ \ \ \ 1\ \ 1\ \ \ \ \ \ \ \ \ \ ] \\
\text{Warp } 2 & [\ \ \ \ \ \ \ \ \ 2\ \ 2\ \ 2\ \ \ \ \ ] \\
\text{Warp } 3 & [\ \ \ \ \ \ \ \ \ \ \ \ \ \ \ 3\ \ 3]
\end{array}
$$

Figure 23: CSR arrays `indices` and `data` and the memory access pattern of the vector CSR SpMV kernel.

divergence in the presence of matrix rows with variable numbers of nonzeros (scalar), or rows with few nonzero elements (vector). It is desireable, then, to have a sparse matrix format and associated computational kernel that is insensitive to sparsity structure. To satisfy these demands we have implemented a COO SpMV kernel based on *segmented reduction*.

Note that `spmv_csr_vector_kernel` (cf. Figure 22) uses a parallel warp-wide reduction to sum per-thread results together. This approach implicitly relies on the fact that each warp processes only one row of the matrix. In contrast, a *segmented* reduction allows warps to span multiple rows. Figure 24 describes our warp-wide segmented reduction, which is the basis of our complete COO kernel (not shown).

Segmented reduction is a data-parallel operation, which like other primitives such as parallel prefix sum (scan), facilitate numerous parallel algorithms [3]. Sengupta *et al.* [17] discuss efficient CUDA implementations of common parallel primitives, including an application of segmented scan to SpMV. Our COO kernel is most closely related to the work of Blelloch *et al.* [4], which demonstrated structure-insensitive SpMV performance the Cray C90 vector computer.

```
__device__ void
segmented_reduction(const int lane, const int * rows, float * vals)
{
    // segmented reduction in shared memory
    if( lane >=  1 && rows[threadIdx.x] == rows[threadIdx.x -  1] )
        vals[threadIdx.x] += vals[threadIdx.x -  1];
    if( lane >=  2 && rows[threadIdx.x] == rows[threadIdx.x -  2] )
        vals[threadIdx.x] += vals[threadIdx.x -  2];
    if( lane >=  4 && rows[threadIdx.x] == rows[threadIdx.x -  4] )
        vals[threadIdx.x] += vals[threadIdx.x -  4];
    if( lane >=  8 && rows[threadIdx.x] == rows[threadIdx.x -  8] )
        vals[threadIdx.x] += vals[threadIdx.x -  8];
    if( lane >= 16 && rows[threadIdx.x] == rows[threadIdx.x - 16] )
        vals[threadIdx.x] += vals[threadIdx.x - 16];
}
```

Figure 24: Parallel segmented reduction is the key component of the COO SpMV kernel.

Figure 25 illustrates the memory access pattern of the COO kernel. Here we have illustrated the case of a single executing warp on a fictitious architecture with four threads per warp. We refer interested readers to the source code which accompanies this paper for further implementation details.

4.5 HYB Kernel

Since the HYB format is simply the sum of its constituent ELL and COO parts, the HYB SpMV operation is trivial to implement. Assuming that most nonzeros belong to the ELL portion, performance of HYB SpMV operation will resemble that of the ELL kernel.

`row`	$\begin{bmatrix}0 & 0 & 1 & 1 & 2 & 2 & 2 & 3 & 3\end{bmatrix}$
`col`	$\begin{bmatrix}0 & 1 & 1 & 2 & 0 & 2 & 3 & 1 & 3\end{bmatrix}$
`data`	$\begin{bmatrix}1 & 7 & 2 & 8 & 5 & 3 & 9 & 6 & 4\end{bmatrix}$
Iteration 0	$\begin{bmatrix}0 & 1 & 2 & 3 & & & & & \end{bmatrix}$
Iteration 1	$\begin{bmatrix} & & & & 0 & 1 & 2 & 3 & \end{bmatrix}$
Iteration 2	$\begin{bmatrix} & & & & & & & & 0\end{bmatrix}$

Figure 25: COO arrays `row`, `col`, and `data` and the memory access pattern of the COO SpMV kernel.

```
__device__ void
process_packet(const int work_per_thread,
               const int   * index_packet,
                     float * data_packet,
               const float * x_local,
                     float * y_local)
{
    for(int i = 0; i < work_per_thread; i++){
        // offset into packet arrays
        int pos = blockDim.x * i + threadIdx.x;

        //row and column indices are packed in one 32-bit word
        int packed_index = index_array[pos];

        // row and column stored in upper and lower half-words
        int row = packed_index >> 16;
        int col = packed_index & 0xFFFF;

        float val = data_array[pos];

        y_local[row] += val * x_local[col];
    }
}
```

Figure 26: A block of threads computes the matrix-vector product for a single packet. Here `x_local` and `y_local` reside in shared memory for low-latency access.

4.6 PKT Kernel

As explained in Section 3.6, the PKT format is comprised by two parts, an array of compressed packets, and a COO matrix containing a smaller number of nonzero values. Since the packet data structure contains an explicit assignment of matrix rows onto a block of threads, processing packets is straightforward. The CUDA code in Figure 26 details steps used to process a single packet using a thread block. Prior to calling `process_packet`, the PKT kernel must load the appropriate sections of the `x` and `y` vectors into the shared memory arrays `x_local` and `y_local` respectively. After processing the packet, the results in `y_local` must be written back to `y`, which resides in global memory. By construction, memory accesses to the PKT data structure, represented by `index_packet` and `data_packet`, are fully coalesced.

4.7 Caching

With the exception of the PKT kernel, which uses a shared memory cache, all SpMV kernels can benefit from the *texture cache* present on all CUDA-capable devices. As shown in the results of Section 5, accessing the `x` vector through the texture cache often improves performance considerably. In the cached variants of our kernels, reads of the form `x[j]` are replaced with a texture fetch instruction `tex1Dfetch(x_tex, j)`,

Kernel	Granularity	Coalescing	Bytes/FLOP (32-bit)	Bytes/FLOP (64-bit)
DIA	thread : row	full	4	8
ELL	thread : row	full	6	10
CSR (scalar)	thread : row	rare	6	10
CSR (vector)	warp : row	partial	6	10
COO	thread : nonzero	full	8	12
HYB	thread : row	full	6	10
PKT	thread : rows	full	4	6

Table 1: Summary of SpMV kernel properties.

leaving the rest of the kernel unchanged.

4.8 Summary

Table 1 summarizes the salient features of our SpMV kernels. For the HYB and PKT entries, we have assumed that only a small number of nonzero values are stored in their COO respective portions. As shown in the column labeled "Granularity", the COO kernel has the finest granularity (one thread per nonzero) while PKT is the coarsest (several rows per thread). Recall that full utilization of the GPU requires many thousands of active threads. Therefore, the finer granularity of the CSR (vector) and COO kernels is advantageous when applied to matrices with a limited number of rows. Note that such matrices are not necessarily small, as the number of nonzero entries per row is still arbitrarily large.

Except for the CSR kernels, all methods benefit from full coalescing when accessing the sparse matrix format. As Figure 21 illustrates, the memory access pattern of the scalar CSR kernel seldom benefits from coalescing. Warps of the vector kernel access the CSR structure in a contiguous but not generally aligned fashion, which implies partial coalescing.

The rightmost columns of Table 1 reflect the computational intensity of the various kernels. As before, we have neglected the COO portion of the HYB and PKT formats. In single precision arithmetic, the DIA and PKT kernels generally have the lowest ratio of bytes per FLOP, and therefore the highest computational intensity. Meanwhile, the COO format, which explicitly stores (uncompressed) row and column entries, has the lowest intensity.

Note that these figures are only rough approximations to the true computational intensities, which are matrix-dependent. Specifically, these estimates ignore accesses to the `y` vector, the `ptr` array of the CSR format, the `offset` array of the DIA format, and the `x` vector used in the PKT kernel. Our matrix-specific bandwidth results in Section 5 provide a more accurate empirical measurement of actual bandwidth usage.

5 Results

We have collected SpMV performance data on a broad collection of matrices representing numerous application areas. Different classes of matrices highlight the strengths and weaknesses of the sparse formats and their associated computational kernels. In this section we explore the effect of these performance tradeoffs in terms of speed of execution, measured in GFLOP/s (billion floating point operations per second), and memory bandwidth utilization, measured in GBytes/s (billion bytes per second).

We present results for both single (32-bit) and double precision (64-bit) floating point arithmetic. In each case, we record performance with and without the caching applied to the `x` vector (cf. Section 4.7). With cache enabled, the reported memory bandwidth figures are the *effective* bandwidth of the computation using the same accounting as the results with no caching. Therefore, effective bandwidth is a hypothetical measure of the memory bandwidth necessary to produce the observed performance in the absence of a cache.

Table 2 lists the software and hardware used in our performance study. All software components, including source code for our implementations, are freely available and the matrices used in our study are available upon

GPU	NVIDIA GeForce GTX 280
CPU	Intel Core 2 Quad Q6600
Memory	2x2GB DDR2-800
Chipset	NVIDIA 780i SLI
OS	Ubuntu 8.04 (Linux 2.6.24-21 x86_64)
CUDA	CUDA 2.1 Beta (2.1.1635-3065709)
Host Compiler	GCC 4.2.4

Table 2: Test platform specifications.

Matrix	Grid	Diagonals	Rows	Columns	Nonzeros
Laplace 3pt	$(1,000,000)$	3	1,000,000	1,000,000	2,999,998
Laplace 5pt	$(1,000)^2$	5	1,000,000	1,000,000	4,996,000
Laplace 7pt	$(100)^3$	7	1,000,000	1,000,000	6,940,000
Laplace 9pt	$(1,000)^2$	9	1,000,000	1,000,000	8,988,004
Laplace 27pt	$(100)^3$	27	1,000,000	1,000,000	26,463,592

Table 3: Structured matrices used for performance testing.

request. The reported figures represent an average (arithmetic mean) of 500 SpMV operations. As described in Section 4, the number of FLOPs for one sparse matrix-vector multiplication is precisely twice the number of nonzeros in the matrix. Therefore, the rate of computation, which is reported in units of GFLOP/s, is simply the number of FLOPs in a single matrix-vector product divided by the average computation time. We do not include time spent transferring data between host and device memory. In the context of iterative solvers, where such transfers would occur at most twice (at the beginning and end of iteration), transfer overhead is amortized over a large number of SpMV operations, rendering it negligible.

5.1 Structured Matrices

We begin with a set of structured matrices that represent common stencil operations on regular one, two, and three-dimensional grids. Our test set consists of standard discretizations of a Laplacian operator in the corresponding dimension. Table 3 lists these matrices and the grid used to produce them. For instance "Laplace 5pt" refers to the standard 5-point finite difference approximation to the two-dimensional Laplacian operator. Note that the number of points in the stencil is precisely the number of occupied matrix diagonals, and, aside from rows corresponding to points on the grid boundaries, it is also the number of nonzero entries per matrix row.

5.1.1 Single Precision

Figure 27 reports SpMV performance using single precision precision arithmetic. HYB results are excluded from our structured matrix study as they are identical to the ELL figures. While the PKT kernel does not use the texture cache, it is included among the cache-enabled kernels for comparison.

As expected, the DIA kernel offers the best performance in all cases. On the 27-point example, the DIA kernel reaches 23.5 GFLOP/s without caching and 36.8 GFLOP/s with caching enabled, an improvement of 56%. ELL performance is similar to DIA, although uniformly slower, owing to reduced computational intensity associated with explicit column indices. Larger stencils, which offer greater opportunity for reuse, see greater benefit from the use of caching with both DIA and ELL.

Despite a competitive computational intensity (cf. Table 1), PKT performance trails that of DIA and ELL. This result is attributable in part to the relatively small size of the shared memory (16KB) which limits the number of rows per packet (approximately 2000). In turn, the number of rows per packet paces a limit

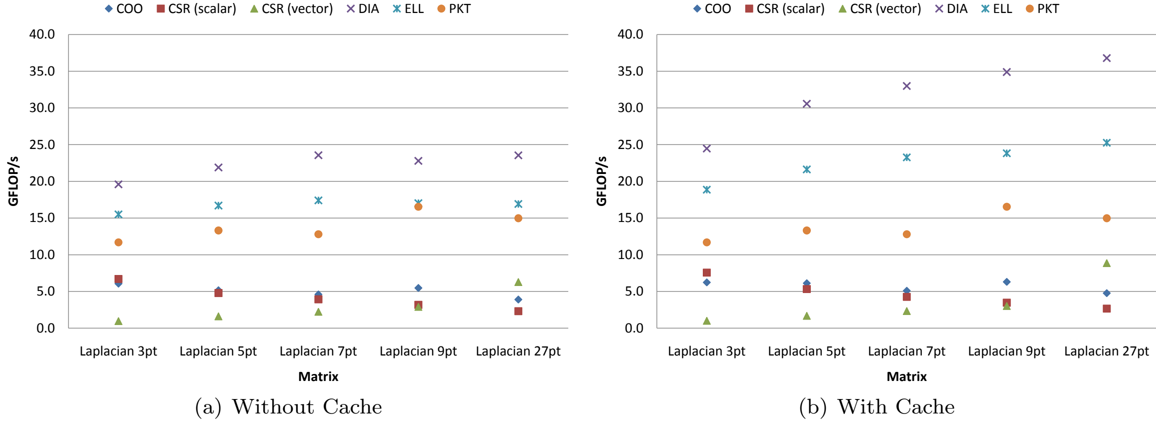

(a) Without Cache

(b) With Cache

Figure 27: Performance results for structured matrices using single precision.

on the number of threads per packet while still maintaining several rows per thread. Our single precision PKT results use 512 threads per packet, or roughly four rows per thread.

Although not competitive with DIA and ELL, the COO kernel exhibits steady performance across the matrices in our study. As shown in Section 5.2, this quality is more important in the context of unstructured matrices. The generality of the COO method is unnecessary for this set of highly regular, grid-based matrices.

Recall from Section 4.3 that the CSR (vector) kernel uses one 32-thread warp per matrix row. Since all matrices in our study have fewer than 32 nonzeros per row, the vector kernel is underutilized. Indeed, when the texture cache is enabled, the ratio of GFLOP/s to nonzeros per row only varies between 0.3285 and 0.3367. That performance scales linearly with the number of nonzeros per row indicates that COO (vector) is entirely limited by poor thread utilization, as opposed to the available memory bandwidth. As a result, the vector kernel is not competitive with DIA and ELL on the matrices considered.

Observe that CSR (scalar) kernel performance decreases as the number of diagonals increases. Given that the number of nonzeros per row varies little, execution divergence of the scalar kernel is minimal. Instead, memory divergence is the cause of the performance decline. The best performance is achieved when the number of nonzeros per row is small, resulting in a modest degree of coalescing. However, as the number of elements per row increases the likelihood of such fortuitous coalescing diminishes. Note that the typical number of nonzeros per row is effectively the same as the stride in the `saxpy` kernels discussed in Section 2. In either case, larger stride is detrimental to performance.

Although GFLOP/s is the primary metric for SpMV performance, it is also instructive to examine memory bandwidth utilization. Figure 28 reports the observed memory bandwidth for each matrix and kernel in our study. The maximum theoretical memory bandwidth of the GTX 280 is 141.7 GBytes/s, and without the aid of caching, the DIA and ELL kernels deliver as much as 76% and 81% of this figure respectively. With caching enabled, the maximum *effective* bandwidth of DIA is 155.1 GByte/s and 156.3 GByte/s for ELL. Of course, these results reflect, in part, the internal memory bandwidth of the device.

5.1.2 Double Precision

Double precision performance and bandwidth results are shown in Figures 29 and 30 respectively. Again the DIA kernel offers the best performance in all cases, reaching 16.7 GFLOP/s on the 27-point example. The ELL kernel runs at 13.5 GFLOP/s on the same matrix.

While the peak rate of double precision computation on the GTX 200-series GPU is an order of magnitude less the single precision maximum, SpMV performance is bandwidth-limited, and therefore insensitive to variations in peak floating point throughput. Indeed, DIA double precision (uncached) performance in the 27-point example is 44.2% that of the single precision result, which nearly matches the ratio of bytes per

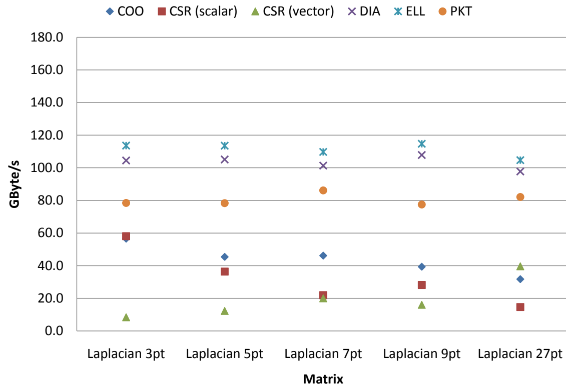

(a) Without Cache

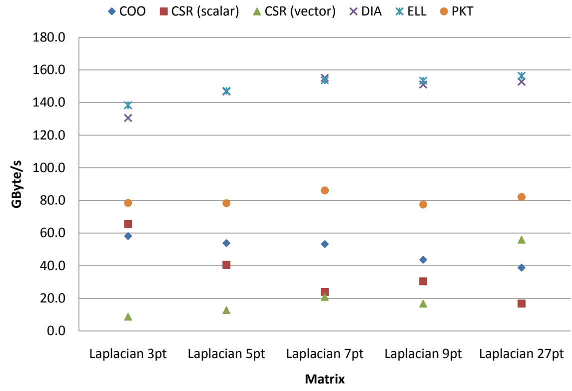

(b) With Cache

Figure 28: Bandwidth results for structured matrices using single precision.

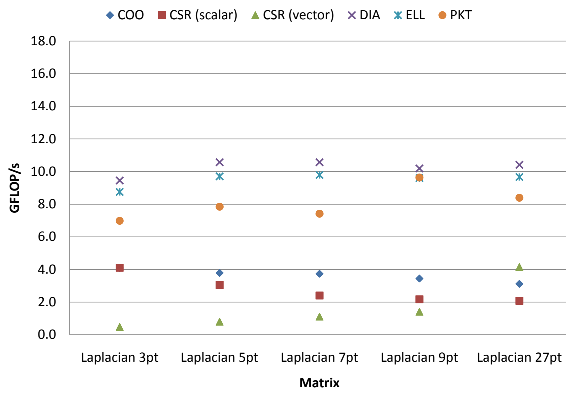

(a) Without Cache

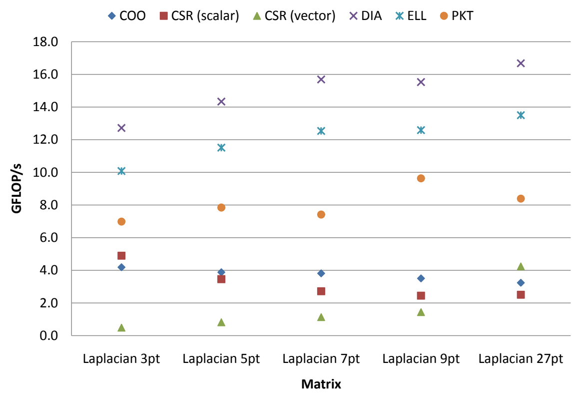

(b) With Cache

Figure 29: Performance results for structured matrices using double precision.

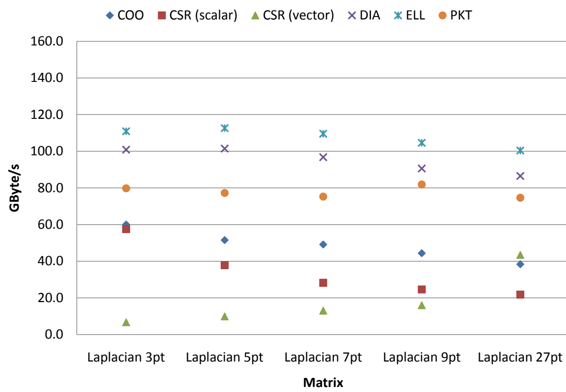

(a) Without Cache

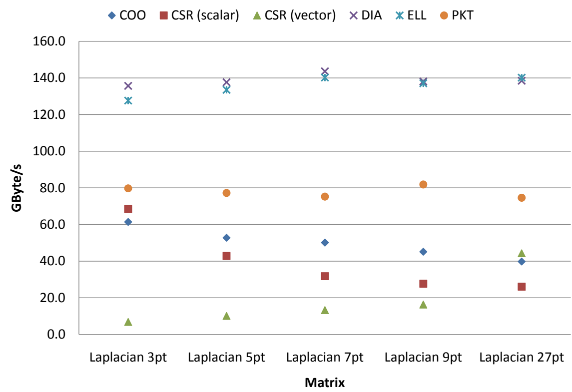

(b) With Cache

Figure 30: Bandwidth results for structured matrices using double precision.

Matrix	Rows	Columns	Nonzeros	Nonzeros/Row
Dense	2,000	2,000	4,000,000	2000.0
Protein	36,417	36,417	4,344,765	119.3
FEM/Spheres	83,334	83,334	6,010,480	72.1
FEM/Cantilever	62,451	62,451	4,007,383	64.1
Wind Tunnel	217,918	217,918	11,634,424	53.3
FEM/Harbor	46,835	46,835	2,374,001	50.6
QCD	49,152	49,152	1,916,928	39.0
FEM/Ship	140,874	140,874	7,813,404	55.4
Economics	206,500	206,500	1,273,389	6.1
Epidemiology	525,825	525,825	2,100,225	3.9
FEM/Accelerator	121,192	121,192	2,624,331	21.6
Circuit	170,998	170,998	958,936	5.6
Webbase	1,000,005	1,000,005	3,105,536	3.1
LP	4,284	1,092,610	11,279,748	2632.9

Table 4: Unstructured matrices used for performance testing.

FLOP of the two kernels (50.0%) as listed in Table 1. For the ELL kernel, a similar analysis suggests a relative performance of 60.0% (double precision to single precision) which again agrees with the 57.2% observed.

Since the remaining kernels are not immediately bandwidth-limited, we cannot expect a direct correspondence between relative performance and computational intensity. In particular, the CSR (scalar) kernel retains 89.9% of its single precision performance, while computational intensity would suggest a 60.0% figure. This anomaly is explained by the fact that uncoalesced double-word memory accesses are inherently more efficient than uncoalesced single-word accesses on a memory bandwidth basis.

5.2 Unstructured Matrices

Our unstructured matrix performance study considers the same corpus of 14 matrices used by Williams *et al.* [19] for benchmarking SpMV performance on several multicore processors. Table 4 lists these matrices and summarizes their basic properties. Further details regarding the origin of each matrix are provided by Williams *et al.* [19].

We have excluded the DIA and ELL formats from our unstructured performance study. Only the Epidemiology matrix is efficiently stored in ELL format, and none are efficiently stored in DIA. While most nonzeros in the Epidemiology matrix are confined to three diagonals, the total number of occupied diagonals is 769.

5.2.1 Single Precision

Single precision SpMV performance is reported in Figure 31. As before, we include the PKT measurements, which do not use the texture cache, in both charts for comparison. Our implementation of the PKT format extends only to matrices with symmetric nonzero patterns, so PKT results for the Webbase and LP matrices are omitted.

Unstructured performance results are varied, with no single kernel or format outperforming all others. The HYB format acheives the highest absolute performance, reaching 22.3 GFLOP/s in the FEM/Spheres example and over 15.0 GFLOP/s in six of fourteen examples. The hybrid format exhibits the worst performance in the LP matrix. As Figure 33 shows, the number of nonzeros per row varies widely in this example from linear programming. In contrast, the distribution of nonzeros per row in the higher-performing Wind Tunnel matrix is more compact. As a result, the only 45.4% of the LP matrix nonzeros are stored in the ELL portion of the HYB data structure while fully 99.4% of the Wind Tunnel nonzeros reside there.

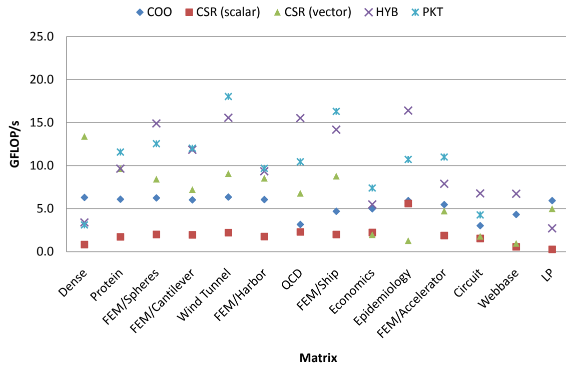

(a) Without Cache

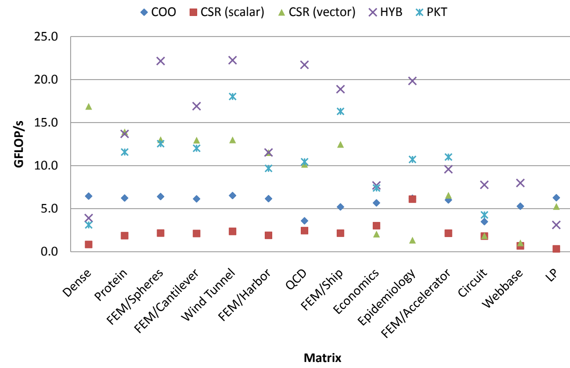

(b) With Cache

Figure 31: Performance results for unstructured matrices using single precision.

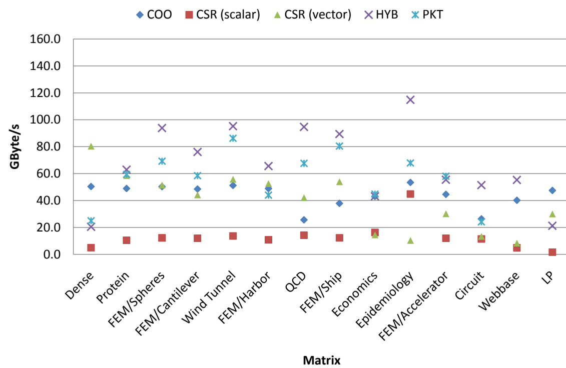

(a) Without Cache

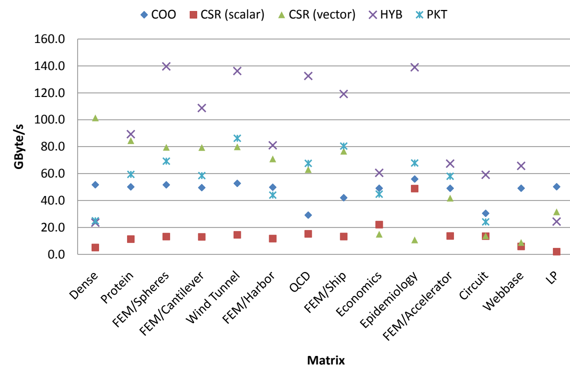

(b) With Cache

Figure 32: Bandwidth results for unstructured matrices using single precision.

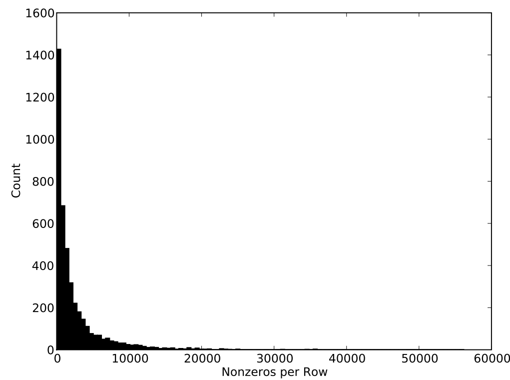

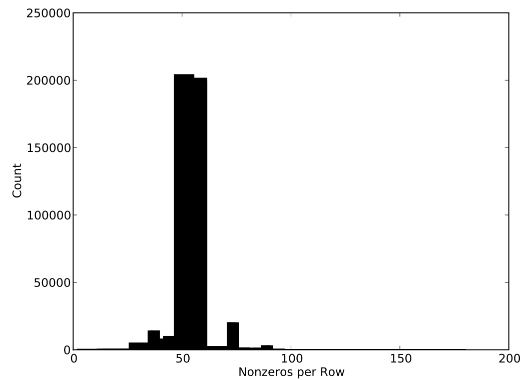

Figure 33: Distribution of number of nonzeros per row for the LP (left) and Wind Tunnel (right) matrices.

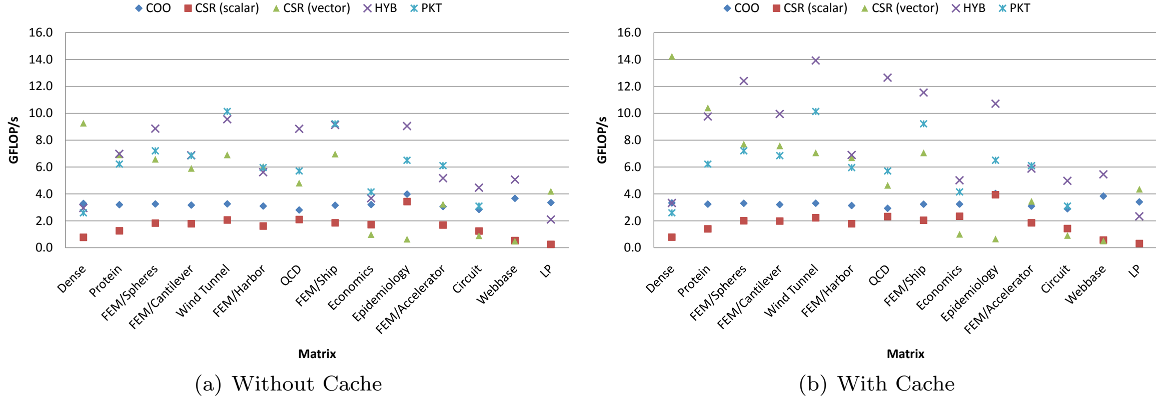

(a) Without Cache

(b) With Cache

Figure 34: Performance results for unstructured matrices using double precision.

It is at first surprising that the HYB format does not perform well on the dense 2,000-by-2,000 matrix. After all, this matrix is ideally suited to the ELL format underlying HYB. Recall from Section 2 that the GTX 200-series processor supports 30K concurrently executing threads. However, the granularity of the ELL kernel (one thread per row) implies that only 2,000 threads will be launched, significantly underutilizing the device. For comparison, applying the HYB kernel to a dense matrix with 30K rows and 128 columns runs at 30.83 GFLOP/s.

The CSR (vector) kernel is significantly faster than HYB on the 2,000 row dense matrix. Here the finer granularity of the vector kernel (one warp per row), decomposes the SpMV operation into 64,000 distinct threads of execution, which is more than sufficient to fill the device. As with the structured matrices considered in Section 5.1, the vector kernel is sensitive to the number of nonzeros per matrix row. On the seven examples with an average of 50 or more nonzeros per row, the vector kernel performs no worse than 12.5 GFLOP/s. Conversely, the matrices with fewer than four nonzeros per row, Epidemiology and Webbase, contribute the worst results, at 1.3 and 1.0 GFLOP/s respectively.

Compared to the other kernels, COO performance is relatively stable across the test cases. The COO kernel performs particularly well on the LP matrix, which proves especially challenging for the other methods. Although LP is the only instance where COO exhibits the best performance, it is clearly a robust fallback for pathological matrices.

The PKT method performs well on finite-element matrices and generally outperforms HYB on this class of problems. However, HYB with caching proves to be a superior combination in all but the FEM/Accelerator example. Therefore, in the cases considered, the texture cache is a viable alternative to explicit precaching with shared memory.

With caching disabled, the memory bandwidth utilization of the HYB kernel (cf. Figure 32) exceeds 90 GByte/s, or 63.5% of the theoretical maximum, on several unstructured matrices. The bandwidth disparity between structured and unstructured cases is primarily attributable to the lack of regular access to the `x` vector. The texture cache mitigates this problem to a degree, improving performance by an average of 30%.

5.2.2 Double Precision

Together, our CSR and HYB kernels surpass the 10.0 GFLOP/s mark in half of the unstructured test cases using double precision values. As shown in Figure 35, the CSR (vector) kernel achieves the highest absolute performance at 14.2 GFLOP/s on the Dense matrix. Wind Tunnel and QCD represent best-case HYB performance at 13.9 and 12.6 GFLOP/s respectively. Again, COO performance is stable, varying from a minimum of 2.9 to a maximum 4.0 GFLOP/s, with most results close to the 3.3 GFLOP/s mark.

The relative performance between double and single precision performance follows the same pattern discussed in Section 5.1.2. The median double precision HYB performance is 62.0% of the corresponding

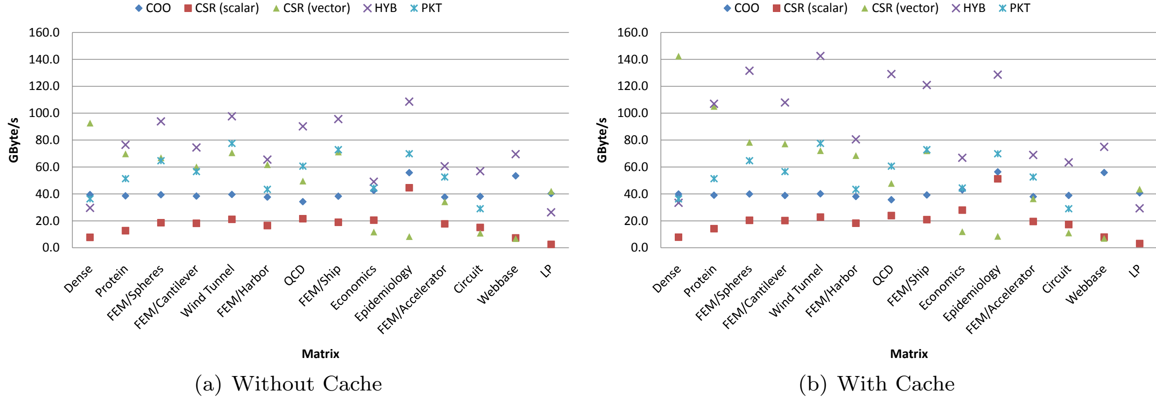

(a) Without Cache (b) With Cache

Figure 35: Bandwidth results for unstructured matrices using double precision.

Name	Sockets	Cores	Clock (GHz)	Description
Cell	1	8 (SPEs)	3.2	IBM QS20 Cell Blade (half)
Opteron	1	2	2.2	AMD Opteron 2214
Xeon	1	4	2.3	Intel Clovertown
Niagara	1	8	1.4	Sun Niagara2
Dual Cell	2	16 (SPEs)	3.2	IBM QS20 Cell Blade (full)
Dual Opteron	2	4	2.2	2 x AMD Opteron 2214
Dual Xeon	2	8	2.3	2 x Intel Clovertown

Table 5: Specifications for several multicore platforms.

single precision result. For CSR (vector), the median is 55.4%. The CSR (scalar) kernel retains 92.1% of its single precision performance, again owing the relative bandwidth efficiency of divergent double-word memory access to single-word accesses.

5.3 Performance Comparison

In this section we provide a comparison between our GPU SpMV results and SpMV results on a variety of multicore architectures. The multicore results were obtained by Williams *et al.* [19], who also provide complete descriptions of each platform. Table 5 summarizes the key features of each platform.

Figure 36 compares double precision SpMV performance of the CSR (vector) and HYB kernels to single and dual socket multicore systems. Examining the single socket platforms we find that the GPU-based methods offer the best performance in all 14 test cases, often by significant margins. Among the other platforms, Cell is the clear winner. It is interesting to note that, like the GTX 200-series GPU, the peak double precision floating point rate of this version of the Cell is a small fraction of its single precision throughput. However, given the memory-bound nature of SpMV, the effective use of memory bandwidth is of much greater importance.

The dual Cell platform is again the fastest of dual socket multicore processors, besting the GPU methods on the FEM/Harbor matrix by a small margin (6.9 GFLOP/s to 7.0 GFLOP/s). In addition to increasing the available memory bandwidth, the addition of a second processor increases the total cache size. As a result, dual socket performance can exhibit super-linear speedup over single socket performance. This effect is most pronounced in the dual socket Xeon platform with 16MB of total L2 cache. Hence, a relatively small matrix like Economics runs four times faster. On the other hand, performance of the dual Xeon system does not scale well on large matrices, such as Wind Tunnel (1.5x faster) and LP (1.3x faster).

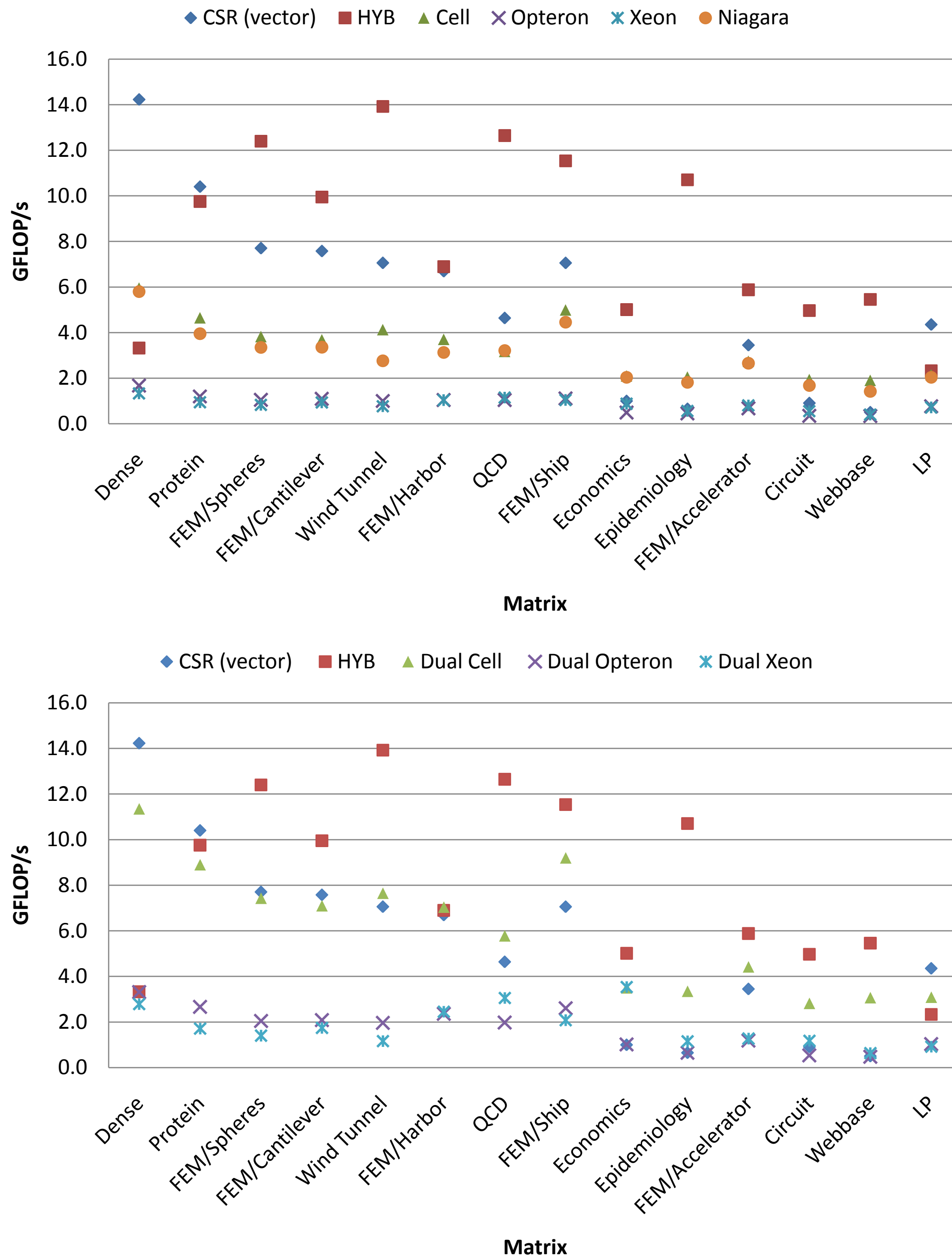

Figure 36: CSR and HYB kernels compared to several single and dual processor multicore platforms.

Figure 37 shows the ratio of the our best GPU kernel performance (either CSR (vector) or HYB) to the performance of the single and dual-processor multicore systems. The median GPU performance advantages over the single socket systems are: 2.47× for Cell, 10.32× for Opteron, 10.85× for Xeon, and 2.79× for Niagara. For dual-processor platforms, the median GPU performance factors are: 1.41× for Cell, 4.96× for Opteron, and 5.33× for Xeon.

6 Conclusion

We have demonstrated several efficient implementations of sparse matrix-vector multiplication (SpMV) in CUDA. Our kernels exploit fine-grained parallelism to effectively utilize the computational resources of the GPU. By tailoring the data access patterns of our kernels to the memory subsystem of the GTX 200-series architecture, we harness a large fraction of the available memory bandwidth. In this section we provide a summary our data structures and SpMV kernels and then close with a brief outline of areas of improvement and topics for future work.

6.1 Results Summary

The DIA and ELL formats are well-suited to matrices obtained from structured grids and semi-structured meshes. DIA is uniformly faster than ELL since both utilize memory bandwidth efficiently and DIA has higher computational intensity. On the other hand, the use of explicit column indices makes ELL a more flexible format.

CSR is a popular, general-purpose sparse matrix format which is convenient for many other sparse matrix computations. A naïve attempt to parallelize CSR SpMV using one thread per matrix row does not benefit from memory coalescing, which consequently results in low bandwidth utilization and poor performance. On the other hand, using a 32-thread warp to process each row ensures contiguous memory access, but leads to a large proportion of idle threads when the number of nonzeros per row is smaller than the warp size. Performance of the scalar method is rarely competitive with alternative choices, while the vector kernel excels on matrices with large row sizes. However, both CSR kernels are subject to execution divergence caused by variations in the distribution of nonzeros per row.

The COO SpMV kernel based on segmented reduction is robust with respect to variations in row sizes and offers consistent performance. However, the COO format is verbose and has the worst computational intensity of the formats considered. Furthermore, the segmented reduction operation more expensive than alternative techniques that rely on a simpler decomposition of work into threads of execution. Nevertheless, the COO kernel is reliable and complements the deficiencies of the other SpMV kernels.

The HYB format, a combination of the ELL and COO sparse matrix data structures, offers the speed of ELL and the flexibility of COO. Often, unstructured matrices that are not efficiently stored in ELL format alone and readily handled by HYB. In such matrices, rows with exceptional lengths contain a relatively small number of the total matrix entries. As a result, HYB is generally the fastest format for a broad class of unstructured matrices. While the PKT format is outperformed by HYB in a majority of cases considered, further improvements are possible.

6.2 Future Work

We have not considered block formats, such as Block CSR or Variable-Block CSR [8] in this paper. Block formats can deliver higher performance [5, 19], particularly for matrices arising in vector-valued problems. A number of the techniques we have applied to scalar formats are compatible with block format extensions.

Special handling for the case of several vectors, so-called *block vectors*, is another standard optimization. In the context of iterative methods for linear systems, this situation occurs when solving for several right-hand-sides simultaneously (i.e. $AX = B$ where B has multiple columns). Furthermore, in the case of eigensolvers such as the LOBPCG [9], it is not uncommon to utilize block vectors with ten or more columns.

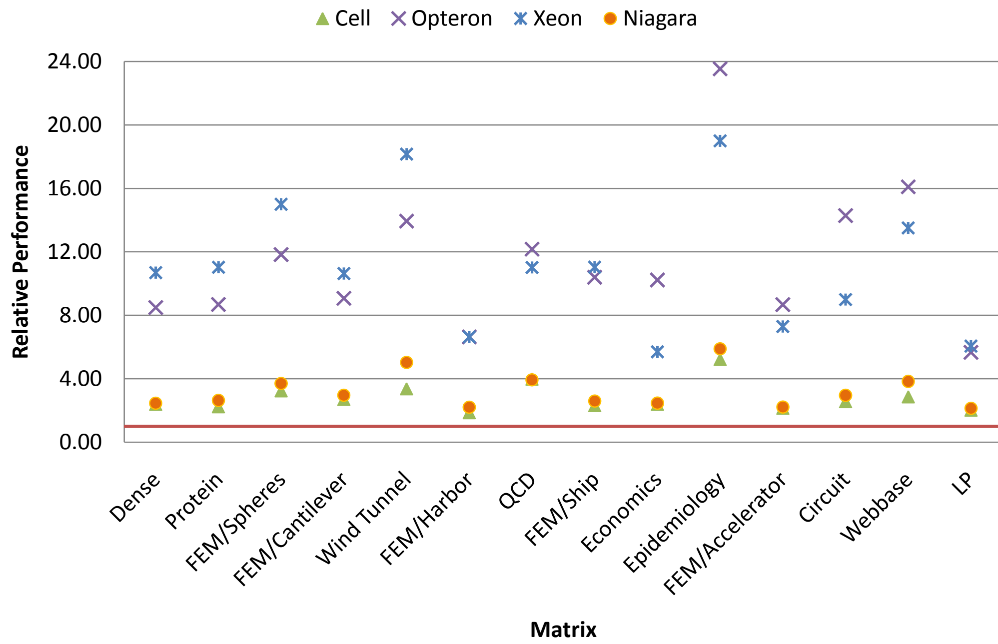

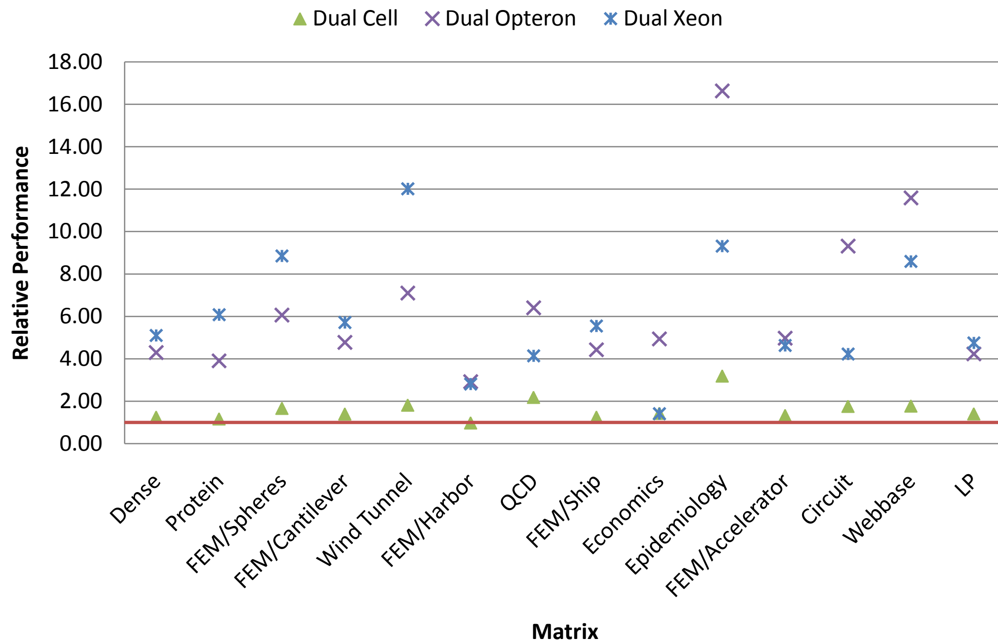

Figure 37: Performance of the best GPU kernel relative to each of the multicore platforms.

Since the memory capacity and performance of any single device, GPU or otherwise, is fixed, it is necessary to distribute large-scale computations over many devices. Effectively decomposing sparse matrix computations over multiple GPUs presents additional challenges, not unlike those faced on distributed memory systems. Tackling these problems, either on a single node with multiple GPUs, or a networked collection of GPU-equipped computers, is an important area of research.

We have only briefly explored the use of shared memory as an explicitly-managed cache. Possible extensions include more sophisticated variations of the packet format or prefetching values used in the CSR kernels. Lastly, alternative packing schemes, such as combining the row, column, and value of a nonzero matrix entry of the COO format into a single multi-word structure, are likely optimizations.

References

[1] E. Anderson, Z. Bai, C. Bischof, S. Blackford, J. Demmel, J. Dongarra, J. Du Croz, A. Greenbaum, S. Hammarling, A. McKenney, and D. Sorensen. *LAPACK Users' Guide*. Society for Industrial and Applied Mathematics, Philadelphia, PA, third edition, 1999.

[2] Sergio Barrachina, Maribel Castillo, Francisco D. Igual, Rafael Mayo, and Enrique S. Quintana-Ortí. Solving dense linear systems on graphics processors. In *Proc. 14th Int'l Euro-Par Conference*, volume 5168 of *Lecture Notes in Computer Science*, pages 739–748. Springer, August 2008.

[3] Guy E. Blelloch. Prefix sums and their applications. Technical Report CMU-CS-90-190, School of Computer Science, Carnegie Mellon University, November 1990.

[4] Guy E. Blelloch, Michael A. Heroux, and Marco Zagha. Segmented operations for sparse matrix computation on vector multiprocessors. Technical Report CMU-CS-93-173, School of Computer Science, Carnegie Mellon University, August 1993.

[5] Luc Buatois, Guillaume Caumon, and Bruno Lévy. Concurrent number cruncher - a GPU implementation of a general sparse linear solver. *International Journal of Parallel, Emergent and Distributed Systems*, to appear.

[6] E.F. DAzevedo, M.R. Fahey, and R.T. Mills. Vectorized sparse matrix multiply for compressed row storage format. In *International Conference on Computational Science (ICCS)*, pages 99–106. Springer, 2005.

[7] R. Grimes, D. Kincaid, and D. Young. ITPACK 2.0 User's Guide. Technical Report CNA-150, Center for Numerical Analysis, University of Texas, August 1979.

[8] Eun-Jin Im, Katherine Yelick, and Richard Vuduc. Sparsity: Optimization framework for sparse matrix kernels. *Int. J. High Perform. Comput. Appl.*, 18(1):135–158, 2004.

[9] Andrew V. Knyazev. Toward the optimal preconditioned eigensolver: Locally optimal block preconditioned conjugate gradient method. *SIAM Journal on Scientific Computing*, 23(2):517–541, 2002.

[10] C. L. Lawson, R. J. Hanson, D. R. Kincaid, and F. T. Krogh. Basic Linear Algebra Subprograms for Fortran Usage. *ACM Transactions on Mathematical Software (TOMS)*, 5(3):308–323, 1979.

[11] J. K. Lenstra, D. B. Shmoys, and É. Tardos. Approximation algorithms for scheduling unrelated parallel machines. *Math. Program.*, 46(3):259–271, 1990.

[12] Erik Lindholm, John Nickolls, Stuart Oberman, and John Montrym. NVIDIA Tesla: A unified graphics and computing architecture. *IEEE Micro*, 28(2):39–55, Mar/Apr 2008.

[13] John Nickolls, Ian Buck, Michael Garland, and Kevin Skadron. Scalable parallel programming with CUDA. *Queue*, 6(2):40–53, Mar/Apr 2008.

[14] NVIDIA Corporation. *NVIDIA CUDA Programming Guide*, June 2008. Version 2.0.

[15] Yousef Saad. SPARSKIT: A basic tool kit for sparse computations; Version 2, June 1994.

[16] Yousef Saad. *Iterative Methods for Sparse Linear Systems*. Society for Industrial Mathematics, 2003.

[17] Shubhabrata Sengupta, Mark Harris, Yao Zhang, and John D. Owens. Scan primitives for GPU computing. In *Graphics Hardware 2007*, pages 97–106. ACM, August 2007.

[18] Vasily Volkov and James W. Demmel. Benchmarking GPUs to tune dense linear algebra. In *Proc. 2008 ACM/IEEE Conference on Supercomputing*, pages 1–11, November 2008.

[19] S. Williams, L. Oliker, R. Vuduc, J. Shalf, K. Yelick, and J. Demmel. Optimization of sparse matrix-vector multiplication on emerging multicore platforms. In *Proc. 2007 ACM/IEEE Conference on Supercomputing*, 2007.